

Vibration reduction and impact resistance experiment on MR absorber system

Zhongchao Deng, Dagang Zhang, Xiongliang Yao

¹ Deepwater Engineering Research Center, Harbin Engineering University, Room701, Ship&Ocean Building, No.145
Nantong Street, Harbin, China, 150001
E-mail: zdeng@deepwatercenter.com

² College of Shipbuilding Engineering, Harbin Engineering University, Room802, Ship&Ocean Building, No.145
Nantong Street, Harbin, China, 150001
E-mail: yaoxingliang@hrbeu.edu.cn

³ Deepwater Engineering Research Center, Harbin Engineering University, Room704, Ship&Ocean Building, No.145
Nantong Street, Harbin, China, 150001
E-mail: dzhang@deepwatercenter.com

Abstract

To reduce low frequency vibration and high frequency impact response at same time is a requirement of modern oil and gas platform. But it is the most of conventional absorber system do not able to do. To address this problem, a new kind of absorber system was presented in this paper. This absorber system consisted of steel wire spring component and Magnetorheological Fluid damper (MR damper) component what were positioned in parallel. The physical experiment results on this absorber system were carried out, it included vibration reduction and impact resistance experiments. Both of the vibration and impact experiments were designed based on MTS hydraulic loading system. The results indicated that the absorber system has a good performance on the system vibration response, the resonance humps of the vibration responses were obviously reduced after using MR damper. For the impact experiment, the absorber system good worked with residual impact response too, but the MR damper's force on impact moment was different from its performance in vibration mode.

Keywords: MR damper; vibration reduction; impact resistance; experiment.

Deepwater Offshore Specialty Symposium, 2009

Introduction

The vibration caused by working equipment and impact from blast accident on offshore platform structure are disadvantages for platform working environment and safety. It should be reduced to as small as possible. For example, when the mud pumps and generators are working, they generate vibrations to the platform and make the working environment to untorable. This vibration should be controlled. Also there could be some explosion accidents on the platforms. It is very important for platform safety to reduce the possible impact on the equipments and working place where the workers are often in. But, the conventional

absorber systems don't able to solve these problems at same time. To address these problems, a new kind of absorber system is presented in this paper. It is composed of wire rope springs and MR (magnetorheological) dampers. The MR dampers and steel rope springs were in parallel position. Fig.1 shows the concept sketch of this system. This absorber system used the advantages of the high and variable damping property of MR damper to make the ship equipments have a good vibration reduction and impact resistance performance.

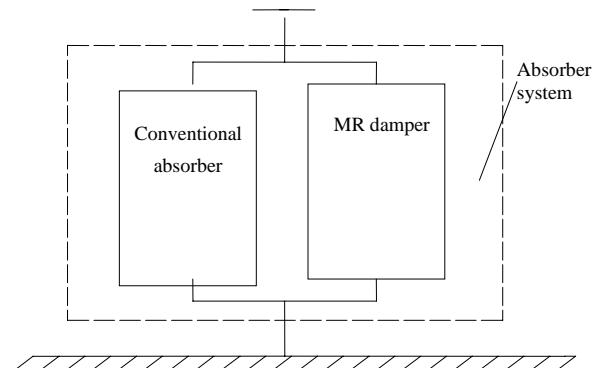


Fig.1 Concept of the absorber system

Over the years, many research results on MR and its applications were carried out. Jinping Ou did experiment for optimizing configuration of a MR damper, and discussed the effect factors on the damping force^[1]. A non-linear model of MR damper was proposed by Ginder, he determined the static yield stress as the maximum shear stress which was modeled as tensile component in the shear direction of the linear infinite single chains of spherical particles^[2]. Carlson proposed that as well as iron-cobalt alloys, iron-nickel alloys in ratio ranging from 90:10 to 99:1 showed a significant increase in the yield stress of MR fluids^[3]. Dyke studied the seismic protection of civil structure using MR damper^[4]. Spencer reported the phenomenological model for MR damper^[5]. A new kind of MR fluid with high yield stress of 100 kPa was reported by

Phule^[6]. The MR fluid effect is often characterized by Bingham Plastic model and its application on vehicle seat was discussed by Sireteanu^[7]. Duan studied the rain-wind-induced cable vibration control on the cable-stayed Dongting Lake Bridge^[8]. Several MR fluid devices have been developed for commercial use by the LORD Corporation.

1 Summary of MR damper and steel rope spring

This absorber system was designed with two main components: MR damper and steel rope spring.

Magnetorheological fluids comprise of a carrier fluid, magneticresponsive particles and surfactants or suspension agents. The particles become polarized in the presence of an applied magnetic field, and organized into chains of particles within the fluid, which increase the apparent viscosity of the fluid. The particles return to an unorganized state when the magnetic field is removed, which lowers the viscosity of the fluid. Fig. 2 illustrates this magnetic phenomenon.

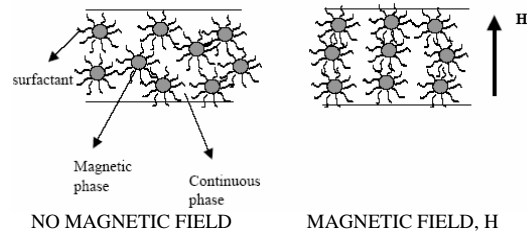


Fig. 2 Sketch of chain-like particles of MR fluids in the magnetic field

MR damper is designed using MR technique. Fig. 3 shows its typical structure sketch. Through changing the current in the loop, the magnetic density in the MR damper will be changed, thus the MR fluid will be in different mechanics characteristic. This makes the MR damper controllable.

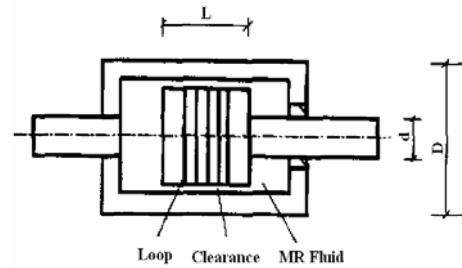


Fig. 3 Sketch of MR damper

MR damper has become a new kind of vibration reduction equipment in the domain of vehicles, machines, bridges, and architectures, etc. with its good characteristics of high damping, great adaptation to temperature, fast response, low energy dissipation, simple structure, and continuously controllable damping. Some MR damper equipments have

been used in practical projects. Currently, research results indicate that the mechanical characteristics of MR damper are related to adscitious magnetic field, displacement amplitude, and excited frequency. Dynamic constitutive relation of MR fluid is very complicated after rheological change. The dynamic damping of MR damper is non-linear.

The MR damper used in this experiment was produced by Harbin Tider Science & Technology Inc. Table 1 is the characteristics and of it.

Table 1 MR damper's characteristics

| Model Number | Maximum Damping Force (kN) | External Diameter (mm) | Install length (mm) | Friction (kN) | Viscosity Coefficient (Pas) | Power (W) |
|--------------|----------------------------|------------------------|---------------------|---------------|-----------------------------|-----------|
| MRD-6-1 | 12 | 120 | 670 | 2.2 | 260 | 20 |

Fig. 4 shows the calibrating test of the MR damper used in this experiment. This calibrating test was used to determine the relationship between damping force, controllable current, and input displacement. It was performed using a MTS hydraulic loading system. In this calibrating test, the movement input signal of the piston of the MR damper was a sinusoid with amplitude of 20 millimeter and period of 2 seconds; the controllable current was from 0 A to 2 A in step of 0.3 A. The damping force of MR damper was obtained by the MTS system automatically.



Fig. 4 MR damper in calibrating test

Fig. 5 illustrates the typical results of MR damper's calibrating test. It shows that the damping force of MR damper increases with the increase of controllable current, and the effect of velocity on the damping force is less.

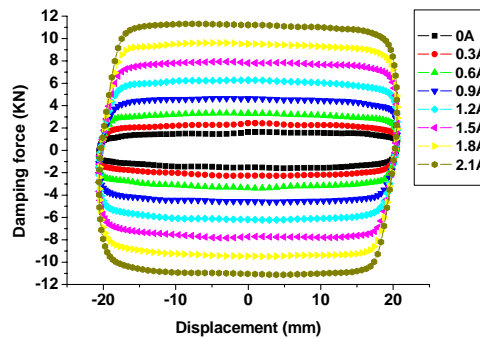


Fig. 5 characteristic curve of MR damper

Steel rope spring is made from steel ropes. Compared with other kind of springs, the steel rope spring has many advantages in practical application, such as lower stiffness, excellent damping performance, lower transmissibility, simple structure, applicability to severe environment, lower cost, etc. Zhanggui Zhong^[9] did the arch steel rope spring experiment, and reported its characteristics. A FEA simulation method for steel rope spring using equivalent young modulus was proposed by Xiongliang Yao^[10].

The steel rope spring used in this experiment was produced by Shanghai Marine Equipment Research Institute. Table 2 is the characteristics of it.

Table 2 Steel rope spring's characteristics

| Model Number | Rated Load (kN) | Dynamic Stiffness (kN/m) | Damping Ratio | Height (mm) | Allowable Deformation (mm) |
|--------------|-----------------|--------------------------|---------------|-------------|----------------------------|
| GSS-2 | 6 | 570 | 0.11 | 120 | 25 |

Fig. 6 shows the calibrating test of the arch steel rope spring used in this experiment. It was performed using an electrical loading system. In this calibrating test, the steel rope spring was pressed by the loading system in force form 0 to 6 kN with a slow velocity of 1 mm/s. Both the force and deformation were obtained by the testing system automatically.



Fig. 6 Steel rope spring in calibrating test

Fig. 7 shows the typical rigidity characteristic curve of the steel rope spring. It shows that the rigidity of the steel rope spring is nonlinear, and it decreases with the increase of the deformation.

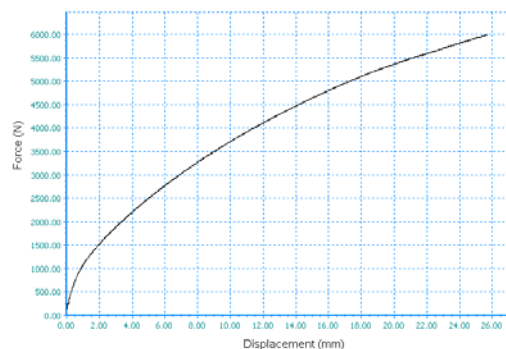


Fig. 7 Characteristic curve of steel rope spring

2 Vibration reduction experiment

2.1 Experiment model and measurement device

The absorber vibration system was simplified as a single degree of freedom system. The dimension parameters of model were determined according to the actual smaller engine. The model scale was 1:1. The maximum model mass was confirmed to be 2000 kg. According to the natural frequency of steel rope spring system about 6 Hz, the steel rope spring equivalent rigidity was determined to be 3600 kN/m. Fig. 8 is the sketch of the experiment model system.

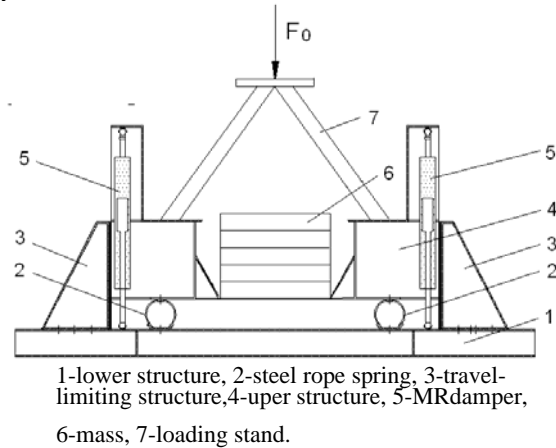


Fig. 8 Sketch of experiment system

The lower structure was used to simulate the base of the equipment, and the upper structure and mass were for the equipment. Lower and upper structures were connected by MR dampers and steel rope springs. There were 4 MR dampers and 6 steel rope springs being used for this model. The travel-limiting structures were used to restrict the horizontal displacement of the upper structure during the experiment. The loading stand was used to apply the exciting load on the model. Fig.9 shows the vibration experiment photo.



Fig. 9 Vibration experiment photo

In the experiment, the force and displacement sensors were used. For each MR damper LR-1 force sensor was installed as shown in Fig.10. And two LC0502 force sensors were used for the middle steel rope spring as shown in Fig. 11. The displacement sensor was located at the center of the model.



Fig. 10 Force sensor of MR damper

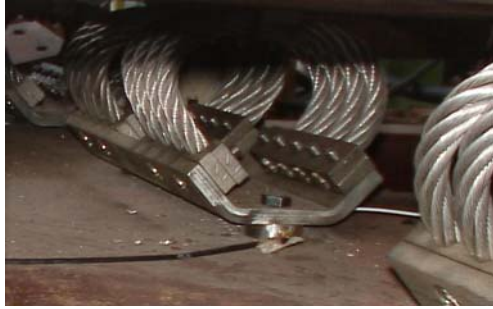


Fig. 11 Force sensor of steel rope spring

The inputs from all sensors were fed to a LMS CADA-X testing and analysis system. It includes a completely digital front end system, SCADAS III, and corresponding analysis software. The response amplitudes were provided by this system through spectrum analysis on the time domain signal.

2.2 Experiment boundary conditions

The main purpose of the vibration experiment is to measure the vibration response under a sinusoidal exciting force. This exciting force was applied to the experiment model using a hydraulic actuator with 10 ton in rated load. The actuator was linked to the model through a supporting stand as shown in Fig. 9.

For the experiment boundary conditions, many load cases were applied in this experiment. These load cases varied in different exciting force amplitude and frequency, different controllable mass, and different damping force of MR dampers. The information of detail load cases is listed below. Each item was in equidifferent range.

Exciting force amplitude: 2 ~12 k N (6 cases)
Exciting force frequency: 1~15 Hz (15 cases)
Controllable mass: 1~2 ton (6 cases)
Controllable current: 0~2 A (8 cases)

2.3 Analysis of experimental results

Fig. 12 and Fig. 13 are the time-displacement history curves of the experiment with controllable mass of 1 ton, exciting force amplitude of 10 kN, and frequency of 1 Hz. The displacement sensors were located on the center of the upper structure. The curves show that the system displacement response was well reduced by this absorber system.

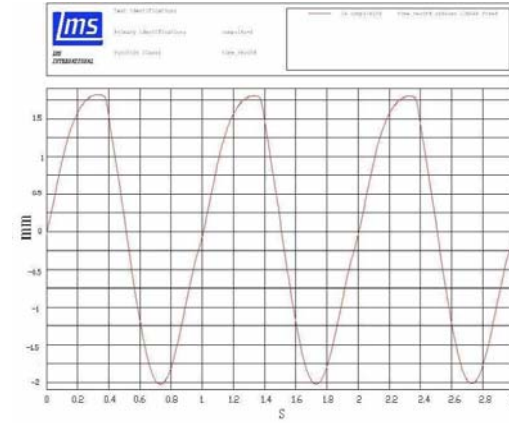


Fig.12 Time-displacement curve at controllable current of 0



Fig.13 Time-displacement curve at controllable current of 2A

For the convenience of describing the vibration experiment results, the nondimensional parameters η , β and λ were used in this paper. The definitions of these parameters are shown in Eqs. 1~3.

Frequency ratio λ was defined as:

$$\lambda = \frac{f}{f_n} \quad (1)$$

Where f is the exciting frequency, and f_n is the natural frequency of the experiment model system. The parameter λ describes the relationship between these two frequencies.

Force transfer ratio η was defined as:

$$\eta = \frac{F_{kc}}{F_0} \quad (2)$$

Where F_{kc} is the resultant force transferred from the MR dampers and the steel rope springs, and F_0 is the corresponding exciting force amplitude.

Nondimensional displacement amplitude ratio β was defined as:

$$\beta = \frac{D}{D_0} \quad (3)$$

Where D is the vibration displacement amplitude induced by the exciting force with amplitude of F_0 , and D_0 is the static displacement under force F_0 .

The parameters η and β describe the vibration reduction effect on force and displacement respectively.

Fig. 14 and Fig. 15 are the typical result curves of this experiment. It shows that the system vibration response was reduced to different lower levels by changing the controllable current of MR dampers. The maximum reduction point of vibration response was at the natural frequency of the vibration system i.e. frequency ratio at 1. The amplitude ratios decreasing of force transferred ratio and nondimensional displacement amplitude ratio are 75% and 71% respectively.

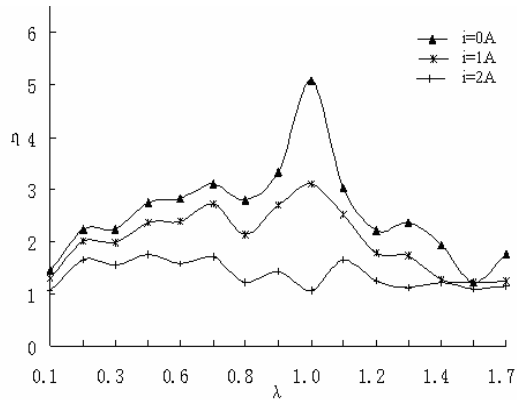


Fig. 14 $\eta - \lambda$ curve with different controllable current

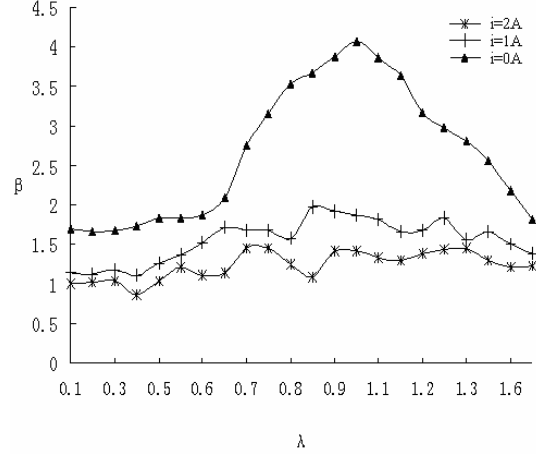


Fig. 15 $\beta - \lambda$ curve with different controllable current

3 Impact experiment

3.1 The boundary conditions

The impact experiment aimed to measure the absorber system's response under the vertical impact loads. The impact loads were applied by a hydraulic actuator through impact loading stand on the lower structure. The rated output force of the actuator is 50t. The impact experiment photo is shown in Fig.12:



Fig.12 The photo of impact experiment

The impact input was determined According to the corresponding impact specification. Fig. 13 shows the acceleration, velocity, and displacement history curves of the impact input. The maximum impact input acceleration was 23 g and the corresponding pulse width was 10 ms.

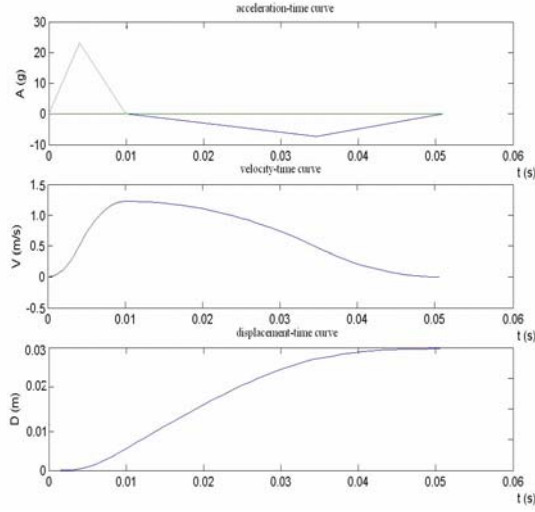


Fig 13 Impact input curves

3.2 Experiment Results Analysis

There were 11 electricity cases in the impact experiment, and they were equidifferented between 0A-2A. The model controllable mass was 2 tons. Fig.14 and Fig.15 show the time domain acceleration input and response respectively.

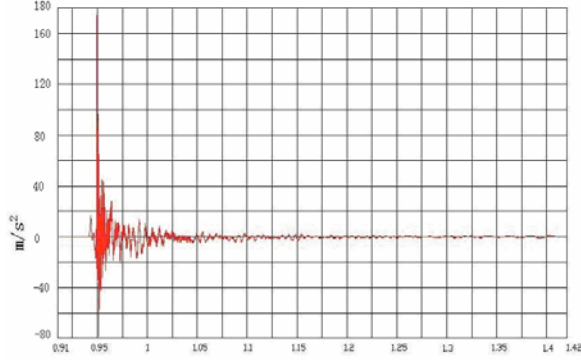


Fig.14 The impact acceleration input

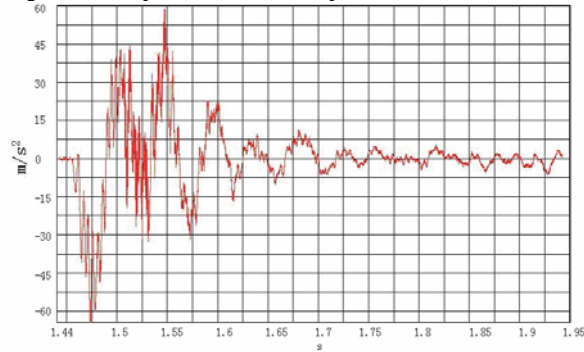


Fig.15 The impact acceleration response

For the convenience of describing the results of the impact experiment, the nondimensional parameters P_a and η_a

were used in this paper. The definitions of these parameters are shown in Eq. 4 and 5.

Acceleration transmissibility P_a is defined as:

$$P_a = \frac{a_o}{a_i} \times 100\% \quad (4)$$

Where a_o is the acceleration peak value of impact response of upper structure, and a_i is the acceleration peak value of impact input on the lower structure. This parameter describes the impact resistance effect on acceleration at the impact moment.

Acceleration attenuation factor η_a is defined as:

$$\eta_a = \frac{a_a}{a_f} \times 100\% \quad (5)$$

Where a_a is the second peak value of the two adjacent waves crest in the acceleration response history, and a_f is the corresponding first peak value. This parameter describes the vibration acceleration attenuation after the impact moment.

Fig. 16 illustrates the relation between acceleration transmissibility and controllable electricity. It showed that the peak values of acceleration didn't have obvious difference in changing the controllable electricity. Tracking the MR damper's force in the experiment indicated that the reason of this phenomenon was that the peak value of the MR dampers' force almost didn't be changed by the controllable electricity during the impact experiment.

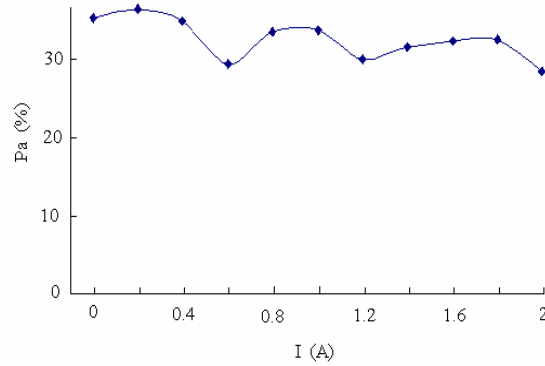


Fig.16 The acceleration transmissibility

The relation between the peak value of MR damper's force and controllable electricity is shown in Fig.17:

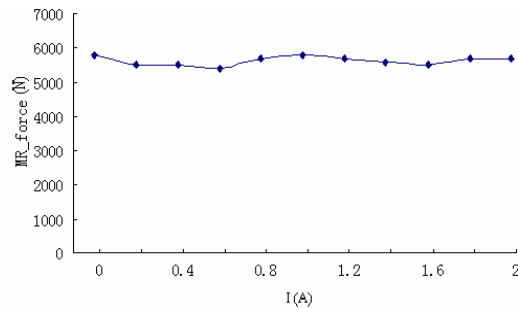


Fig.17 peak value of MR force with control current

Fig.17 shows that in the impact experiment, the MR damper showed a big different characteristic compared to its performance in the vibration experiment. The MR damper's force almost was not changed by changing controllable electricity. MR damper's impact mathematics model should be different to the vibration model.

Fig. 18 illustrates the relationship between acceleration attenuation factor and controllable electricity.

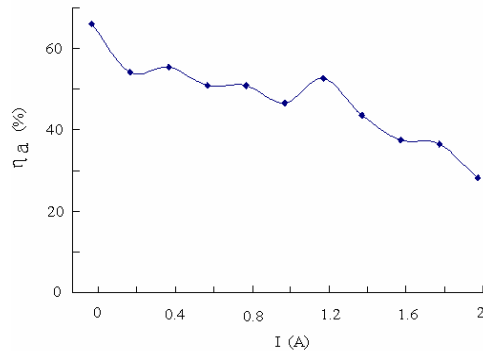


Fig.18 velocity damping factor

It shows that the acceleration attenuation factor became smaller with the increase of controllable electricity. According to the definition of the acceleration attenuation factor, it's clear that the bigger the system damping, the smaller the attenuation factor. So this experiment phenomenon shows that the MR damper has a good effect on the vibration after impact like in the vibration experiment.

CONCLUSIONS

In the scope of this study, the vibration and impact experiment on this absorber system was carried out. The results show that:

The absorber system based on MR damper has good effect on vibration reduction in low frequency. The optimal vibration reduction point was at controllable current was 2A, the force transferred ratios under all of the exiting frequency were near to 1. The vibration response is controlled evidently, especially at the system natural frequency, the resonance hump of the vibration response

was obviously reduced, and the reduction of vibration response can reach 71%. For impact experiment, the MR damper's performance had a little difference with that it performed in vibration experiment. At the impact moment, the MR damper's force was approximately constant, and wasn't changed with the changing controllable electricity obviously. But the MR damper's effect on the residual vibration after the impact moment was as good as in the vibration experiment.

Acknowledgement

The authors of this paper gratefully acknowledge the 111 project for their support in preparing this paper.

References

- [1] JOU J P, GUAN X C. Experimental Study of Magnetorheological Damper Performance[J]. Earthquake Engineering and Engineering Vibration, 1994, 18(3):74-81.
- [2] GINDER J M, DAVIS L C, ELIE L D. Rheology of Magnetorheological Fluids: Models and Measurements[C]//: 5th Int. Conf. on ERF, MRS and Their Applications, UK: Univ. Sheffield, 1995, 504-514.
- [3] CARLSON J D, WEISS K D. Magnetorheological Materials Based on Alloy Particles[P]. U.S. Patent, 1995, No 5,382,373.
- [4] DYKE S J, SPENCER B F, SAIN M K, CARLSON J D. Seismic Response Reduction Using Magnetorheological Dampers[C]//: Proc. of the IFAC World Congress, San Francisco, CA, 1996, 145-150.
- [5] SPENCER B F. Phenomenological model for magnetorheological damper[J]. J. Engrg. Mech., ASCE, 1997, 123(3):230-238.
- [6] PHULE P P, GINDER J M. Synthesis of Novel Magnetorheological Fluids[J]. MRS Bulletin, 1998, 23(8):23-25.
- [7] SIRETEANU T, STANCIOIU D, STAMMERS C W. Use of Magnetorheological fluid dampers in semi-active driver seat vibration control[C]. ACTIVE 2002, ISVR, Southampton, UK, 2002.
- [8] DUAN Y F, NI Y Q, KO J M. Cable Vibration Control using Magnetorheological Dampers[J]. Journal of Intelligent Material Systems and Structures, 2006, 17(4):321-325.
- [9] ZHONG, Z. Low-frequency Big-damping and Impact-resistance Absorber of Arch Steel Wire Spring[J]. Ship Engineering, 2005, 15(1):16-22.
- [10] YAO X L. Ship Vibration[M]. Harbin Engineering University Publishing Company, 2004: 51-66.